Tunable Single-Atomic Charge/Spin States of Intercalant Co Ions in a Transition Metal Dichalcogenide

Seongjoon Lim
Rutgers Center for Emergent Materials and Department of Physics and Astronomy, Piscataway, NJ 08854, USA https://orcid.org/0000-0002-8383-5534

Shangke Pan
State Key Laboratory Base of Novel Function Materials and Preparation Science, School of Material Sciences and Chemical Engineering, Ningbo University

Kefeng Wang
University of Maryland

Alexey Ushakov
Institute of Metal Physics, S. Kovalevskaya Street 18, Yekaterinburg

Ekaterina Sukhanova
Emanuel Institute of Biochemical Physics of RAS, 4 Kosygin Street, 119334, Moscow

Zakhar Popov
National University of Science and Technology MISiS https://orcid.org/0000-0003-4882-401X

Dmitry Kvashnin
Emanuel Institute of Biochemical Physics https://orcid.org/0000-0003-3320-6657

Sergey Streltsov
Institute of Metal Physics, S. Kovalevskaya Street 18, Yekaterinburg https://orcid.org/0000-0002-2823-1754

Sang-Wook Cheong (sangc@physics.rutgers.edu)
Rutgers Center for Emergent Materials and Department of Physics and Astronomy
https://orcid.org/0000-0001-9905-6175

Article

Keywords: two-dimensional (2D) materials, intercalation, electronics, spintronics

Posted Date: July 19th, 2021

DOI: https://doi.org/10.21203/rs.3.rs-647929/v1

Abstract

Intercalation raises manifold possibilities to manipulate the properties of two-dimensional (2D) materials[1], and its impact on local electronic/magnetic properties has drawn much attention with the rise of nano-structured 2D materials[2,3]. Typically, changing an ionic state in a solid involves a dramatic local change of energy as well as orbital/spin magnetic moment from its ground state. However, the atomic investigation of the charging process of an intercalant ion in 2D material has never been explored while such subject has been studied in artificially deposited atoms on thin insulating 2D layers using scanning probe microscopy[4–7]. Herein, we demonstrate an atomical manipulation of the charge and spin state of Co ions on a metallic NbS_2, obtained by cleaving of Co-intercalated NbS_2. Density functional theory investigation of various Co configurations reveals that the charging is possible due to a change in the crystal field at the surface and a significant coupling between NbS_2 and intercalants occurs via orbitals of the a_{1g} symmetry. The results can be generalized to numerous other combinations of intercalants and base matrixes, suggesting that intercalated transition metal dichalcogenides can be a new platform to introduce single-atom operation 2D electronics/spintronics.

Main Text

Intercalation has long been studied as a strategy to derive various properties from graphene[8], and the examples span from the practical use of lithium intercalation in battery[9] to the non-trivial intercalation-induced superconductivity[10,11]. With the advent of transition metal dichalcogenides (TMD) in 2D spintronics[12] as a bridging material between two principal components, i.e. graphene and hexagonal boron nitride, intercalation has been adopted in TMD as well to derive various emergent properties, such as generation of magnetic order with self-intercalation[13], controlled doping[3], rectification of thermal conduction[14], catalytic efficiency in hydrogen evolution reaction[15], Z_3 Potts-nematic antiferromagnetism[16], and electrically switchable magnetic order[17]. Despite the diverse combinations of intercalant and base matrix, TMDs intercalated with 3d transition metals are of particular interest due to their great tunability in various magnetic ground states such as ferromagnetic[18–20], antiferromagnetic[21], or helical magnetism[22,23]. They have several distinguished properties such as the localized intercalant *d*-orbital state within the delocalized state of the matrix[24,25] and distinguished magnetic critical behavior[26]. Moreover, remarkable properties such as anomalous hall effect[20,21,27] or spontaneous spin-polarized electric conduction[28] suggest potential discovery of non-trivial phenomena with atomic investigation of intercalants in 3d metal intercalated TMDs.

In this report, we show that a Co ion on a cleaved surface of intercalated $Co_{1/3}NbS_2$ can exhibit a metastable charged state distinguished from other structural defect states. The metastable charged state can be controlled using scanning tunneling microscopy (STM) probe, which resulted in manipulation of charge and spin states of Co ion. Although the process is similar to what have been reported in single electron charging of deposited atom on thin insulating film[4], the absence of insulating layer, which is the

essential part of various charge manipulation experiments[4–7], contrasts the fundamental difference of the process. The existence of van der Waals gap in the bulk structure seems involved in reducing coupling of the intercalated ion orbitals from the base matrix states even without any further insulating layer in between. We have performed density functional theory (DFT) calculations to understand the intriguing existence of the metastable charged state on the metallic substrate and revealed that the reduction of crystal field on the surface and subsequent shift of localized a_{1g} orbital towards the Fermi level play a role in making the localized state accessible by the STM tip. The result demonstrates the smallest structure in which a single charged ion can exist on a metallic compound by adopting intercalation into 2D TMD material and can be a new pathway to incorporate electronic/magnetic control over various 2D materials.

$Co_{1/3}NbS_2$ is an intercalated version of metallic NbS_2 where the Co ions occupy one third of Nb atop sites within the van der Waals gap as in Fig. 1a. The intercalant position alternates between two columns along *c* axis which produces two thirds of Nb ions in Wyckoff 4f sites while one third of Nb sites remain 2a sites. As a result, Co ions form a triangular lattice within one van der Waals gap and they tend to remain on one surface when the crystal is cleaved at low temperature (see methods for details). For convenience, we will refer each layer from the cleaved surface towards bulk with numbers as indicated in Fig. 1a, e.g. layer 1 Co, layer 2 S, layer 3 Nb, etc. Fig. 1b shows an STM topography of a cleaved $Co_{1/3}NbS_2$ surface terminated with Co. In comparison with the simulated STM image showing the ideal trigonal lattice of Co ions (Fig. 1b inset), the STM image shows the existence of various types of defects. Exhaustive DFT calculations make it possible to determine the exact atomic structure of all defect types. The most frequent defects are single/double Co vacancies in layer 1 (Fig. 1c and d), Co substitution of Nb in layer 3 (Fig. 1e), and Co trivacancy in layer 5 (Fig. 1f). Simulated STM images for described defects in Fig. 1c-f as well as other structural defect types are presented in Supplementary Information (SI, discussion in SI section 2).

We should pay additional attention to one feature in STM images, shown in Fig. 1g, which deserves a special consideration. First, it does not fit to any structural model and more importantly it is metastable and degrades with time (see below). It is clearly distinguished from other defects in the extent of vertical/lateral expansion as indicated in Fig. 1h (red solid circle: metastable state, Fig. S13 in SI). We explored the origin of these metastable states by means of DFT+U+(SOC) calculations, which also provide other important information. E.g. they show that the electronic structure of Co in layers 1 (i.e. at surface) and 5 (internal layer) is very different (Fig. 2a). The latter has 2+ ($3d^7$) high-spin state with *S=3/2* (Fig. 2d) similar to the reported Co valency of 2+ in the bulk measurement[29]. It is in contrast to what we have at the surface. Detailed analysis of occupation matrix unambiguously demonstrates that Co in layer 1 is 1+ ($3d^8$, *S=1*) with additional electron at the a_{1g} orbital (Fig. 2e) and its local magnetic moment is 1.93 . This is due to the specific surface termination where only three of S ions remain out of initial CoS_6 octahedron. As a result the t_{2g}-e_g crystal-field splitting for surface Co practically vanishes: projecting DFT Hamiltonian onto the Co *3d* Wannier-functions[30] we find that it reduces from ~1.2 eV in bulk down to ~0.3 eV for Co at the surface. The reduction stimulates occupation of the Co a_{1g} states and leads to

redistribution of electrons at the surface, so that these Co turn out to be closer to 1+ oxidation state. Importantly the hybridization between Nb $3z^2$-r^2 and Co a_{1g} orbitals (directed to each other as in Fig. 2b) pins the latter at the Fermi level and makes it accessible for STM.

Moreover, while surface Co ions are 1+ in the ground state, the Co^{2+} high-spin configuration is also locally stable, and it is rather close in energy. The total energy of such metastable state is only 130 meV/Co higher than the ground state. Other possible metastable configurations are low-spin ($S=0$) Co^{1+} and ($S=1/2$) Co^{2+} states; however, analysis of calculations shows that such states are locally unstable (stable only at corresponding constraints) and energetically much higher than the ground state. The instability of these configurations can be naturally explained by a large intra-atomic Hund's exchange for Co ($J_H \sim 1$ eV[31]) and non-zero exchange field due to Co ions in deeper layers.

It is important that the metastable state of surface Co with the different charge and magnetic state is not only locally stable, but also in the energy range accessible for its switching by STM. To check this hypothesis, we used a STM tip with a combination of various tip heights and biases to induce the metastable surface Co^{2+} state. Fig. 3a illustrates the optimal charging procedure that could successfully induce the metastable charged state. After locating the tip on top of the target Co ion, the tip height is lowered by changing setpoint current to 100 pA which is higher than the normal imaging condition, 10 pA at 5 mV. It is followed by a bias voltage pulse to the tip which is kept at 150 mV for 300 ms indicated by the red stars in Fig. 3a.

We could confirm creation of the metastable charged state by subsequent tunneling current change as well as from STM images showing created Co^{2+} ions having the same height profile with the naturally found ones. Fig. 3b-g show a series of STM images taken on an area while we apply pulses in between. The points marked with red stars in each image were applied a voltage pulse immediately right after, and then the targeted Co ion becomes a metastable charged Co^{2+} showing bright protrusion in the next image. For example, we applied the pulse to the red starred point in Fig. 3b right after the image, then the following Fig. 3c shows a bright metastable charged state at the position. Similarly, we used two pulses after Fig. 3c that resulted in producing the two bright Co ions in Fig. 3d, and so on. One interesting point is that the first charged Co has returned to the ground state between Fig. 3e and f (black dashed circle), but the point was charged again by applying another pulse after Fig. 3f, which demonstrates its bistable nature.

To estimate the overall lifetime of the charged state, we have performed a charging experiment on a massive number of Co sites, and it was estimated to be 43 min (SI section 3.1). The measured lifetime is very unusual compared to Au charging on NaCl/Cu[32] that requires two or more insulating layers to obtain an hour-long lifetime, or donor state in a semiconductor that exists only under tip induced band (i.e., zero lifetime)[33]. The discovery of the intriguing role of van der Waals gap in inducing orbital separation between intercalant and metallic base can be of particular importance in this study. Besides that, we were able to see that the lifetime of the charged state varies a lot by its environment, and the extreme case is

when the charged state is in the vicinity of Co vacancies where they show frequent changes within a single frame of STM image as shown in red dashed circles in Fig. 1h. It implies that an even longer-lived charged state can be obtained by controlling the number of structural defects in the crystal. The result opens the possibility of switching the Co d^7-d^8 states[34] with unprecedented lifetime on a conducting substrate.

Another unique aspect of the charging process is that we could induce the change in both of bias polarities as shown schematically in Fig. 4a. When the sample bias is positive, a single electron hopping happens from the Co ion to the sample as the direction of tunneling electrons. On the other hand, when the sample bias is negative, the direction of tunneling current is reversed and likewise the single electron hopping occurs towards the tip. However, the change of Co is always from Co^{1+} to Co^{2+} by losing one electron. It is in contrast with the case of single atom on insulating NaCl layer[4,35] which shows suppressed electron hopping towards the sample by the presence of insulating layer and gets an electron only from tip. Thus, the bi-polarity nature of the process is another illustration of the fact that the localized Co *3d* electrons at surface are coupled somewhat with the rest of metallic sample. In order to compare the electron hopping probability towards tip and sample, we compared the time to generate a charged Co^{2+} in both polarities. (SI Table S1) The estimated numbers of tunneling electrons to provoke charged state are measured to be and electrons for the tunneling towards tip and sample, respectively (at normalized tunneling current of 300 pA with sample biases of ±200 mV). Considering that the hopping rate towards the tip can be tuned by adjusting the vacuum gap, those comparable rates imply the possibility of fine tuning between electron hopping towards tip and sample.

Lastly, we demonstrate formation of a linear chain of *S=3/2* Co^{2+} ions through Fig. 4b-g. Fig. 4g shows the final result of eight consecutive *S=3/2* Co^{2+} chain and interestingly the charging pulses were applied twice for the first and seventh Co ions as they have changed back to the ground state during the process. In principle, the procedure can be adopted to arrange *S=3/2* Co^{2+} ions of any desired shape in background *S=1/2* Co^{1+} lattice unless the system has low enough defect density. As the procedure can arrange ions with different magnetic moment freely, a cleaved surface of $Co_{1/3}NbS_2$ can be an interesting playground to study the interactions among various arrangements of ions with different magnetic moments.

In summary, we have shown that one can atomically tune the charge and spin state of intercalant Co ions from a cleaved surface of $Co_{1/3}NbS_2$ by STM. It is possible because of the reduced t_{2g}-e_g crystal-field splitting of surface Co as well as the decoupled nature of the intercalant orbitals from its matrix. The metastable Co^{2+} high-spin state turns out to be long-lived and transforms to ground state up to a time scale of ~ 43 minutes, which is extraordinarily long for an ion placed on a metallic substrate. In contrast to the previously reported single atom-type charging processes a whole lattice of switchable Co ions is available in the case of $Co_{1/3}NbS_2$ and its combination with metallic internal layers can be potentially useful for spintronics. Finally, $Co_{1/3}NbS_2$ is just one example of a large family of intercalated TMDs, which can have a different intercalated transition metal, varying degree of intercalation, or a choice of

intercalation host, with a potentially similar atomic tunability with different combinations of spin and charge states.

Methods

Crystal growth

Single crystalline $Co_{1/3}NbS_2$ samples were synthesized by chemical vapor transport method using iodine transport agent. Co rich molar ratio of Co:Nb:S=7:10:20 was used to tune the final composition to $Co_{1/3}NbS_2$ characterized by energy dispersive x-ray analysis. The 0.2 g of mixture together with 0.1 g of iodine were sealed in a quartz tube under vacuum and placed in a two-zone furnace. The set point temperatures of the two zones were 800°C and 950°C, which were kept for 4 weeks. Hexagonal shaped single crystals were collected after cooling the furnace to room temperature.

Scanning Tunneling Microscopy

$Co_{1/3}NbS_2$ samples were fixed to a CuBe sample plate and a metal post was attached to the top surface with Epotek H20E epoxy. The cured samples were transferred to the ultra-high vacuum chamber and inserted to the cleaving stage. The sample was cooled at the stage by liquid nitrogen for 30 mins prior to cleaving and moved to the STM head right after removal of the metal post. STM measurements were performed using USM-1500 SPM system from Unisoku operated with Nanonis controller. The tips were characterized on sputter/anneal cleaned Cu(111) sample prior to use. All the STM measurements are measured at 78 K.

DFT Calculation and STM Simulation

The investigation of the $Co_{1/3}NbS_2$ was carried out within the framework of density functional theory (DFT)[36] implemented in computational package VASP[37–39]. The generalized gradient approximation in form of Ref. 40 was used. All calculations were carried out with the use of the projector-augmented wave (PAW)[41] basis set technique. To consider strong electronic correlations GGA+U[42] method was used. We chose the on-site Coulomb repulsion parameter for Co to be U = 6 eV, while the Hund's rule coupling parameter (J_H) was taken as J_H = 1 eV[31]. The energy cutoff of plane waves was chosen to be 500 eV. The integration over the first Brillouin zone was performed according to Monkhorst-Pack scheme[43] with the density of k-point being equal to 0.014 2π/Å. The electron population numbers were obtained by integration within atomic spheres with radii 1.302 Å, 1.503 Å, and 1.164 Å for Co, Nb and S correspondingly around each atom. The atomic structure relaxation was carried out until the maximum value of interatomic forces became less than $5•10^{-3}$ eV/Å, and the energy variation between two steps of electronic loop became less than $1•10^{-5}$ eV. To avoid an artificial interaction between structures in non-periodic directions a vacuum region of at least 15 Å was chosen. The simulated STM images of all considered structures were obtained by Hive software[44] based on the Tersoff-Hamann approximation[45]. For more calculation details see Supplementary Information Section 1.

Declarations

Author contributions

S.L. performed the STM measurement. S.P. and K.W. were responsible for growth. A.V.U., S.V.S, and E.V.S. performed DFT calculations, E.V.S., Z.I.P., and D.G.K. carried out the STM simulations. S.L., S.V.S., and S.W.C. co-wrote the paper, and all authors revised the manuscript. All authors discussed the results and S.W.C. supervised the whole work.

Acknowledgement

This work was supported by the center for Quantum Materials Synthesis (cQMS), funded by the Gordon and Betty Moore Foundation's EPiQS initiative through grant GBMF6402 and by Rutgers University. DFT calculations were supported by the Russian Science Foundation via RSF 20-62-46047 project, while simulation of STM patterns was funded by RFBR and SC RA, project number 20-53-05009.

References

1. Wang, Z., Li, R., Su, C. & Loh, K. P. Intercalated phases of transition metal dichalcogenides. *SmartMat* **1**, (2020).

2. Wan, J. *et al.* Tuning two-dimensional nanomaterials by intercalation: materials, properties and applications. *Chem. Soc. Rev.* **45**, 6742–6765 (2016).

3. Gong, Y. *et al.* Spatially controlled doping of two-dimensional SnS2 through intercalation for electronics. *Nature Nanotechnology* **13**, 294–299 (2018).

4. Repp, J., Meyer, G., Olsson, F. E. & Persson, M. Controlling the Charge State of Individual Gold Adatoms. *Science* **305**, 493–495 (2004).

5. Patera, L. L., Queck, F., Scheuerer, P. & Repp, J. Mapping orbital changes upon electron transfer with tunnelling microscopy on insulators. *Nature* **566**, 245–248 (2019).

6. Scheuerer, P. *et al.* Charge-Induced Structural Changes in a Single Molecule Investigated by Atomic Force Microscopy. *Phys. Rev. Lett.* **123**, 066001 (2019).

7. Scheuerer, P., Patera, L. L. & Repp, J. Manipulating and Probing the Distribution of Excess Electrons in an Electrically Isolated Self-Assembled Molecular Structure. *Nano Lett.* **20**, 1839–1845 (2020).

8. Dresselhaus, M. S. & Dresselhaus, G. Intercalation compounds of graphite. *Advances in Physics* **51**, 1–186 (2002).

9. Li, Y., Lu, Y., Adelhelm, P., Titirici, M.-M. & Hu, Y.-S. Intercalation chemistry of graphite: alkali metal ions and beyond. *Chem. Soc. Rev.* **48**, 4655–4687 (2019).

10. Csányi, G., Littlewood, P. B., Nevidomskyy, A. H., Pickard, C. J. & Simons, B. D. The role of the interlayer state in the electronic structure of superconducting graphite intercalated compounds. *Nature Physics* **1**, 42–45 (2005).

11. Hannay, N. B. *et al.* Superconductivity in Graphitic Compounds. *Phys. Rev. Lett.* **14**, 225–226 (1965).

12. Avsar, A. *et al.* Colloquium: Spintronics in graphene and other two-dimensional materials. *Rev. Mod. Phys.* **92**, 021003 (2020).

13. Zhao, X. *et al.* Engineering covalently bonded 2D layered materials by self-intercalation. *Nature* **581**, 171–177 (2020).

14. Li, B. *et al.* Liquid-like thermal conduction in intercalated layered crystalline solids. *Nature Materials* **17**, 226–230 (2018).

15. Yang, J. *et al.* Ultrahigh-current-density niobium disulfide catalysts for hydrogen evolution. *Nature Materials* **18**, 1309–1314 (2019).

16. Little, A. *et al.* Three-state nematicity in the triangular lattice antiferromagnet Fe 1/3 NbS 2. *Nature Materials* **19**, 1062–1067 (2020).

17. Nair, N. L. *et al.* Electrical switching in a magnetically intercalated transition metal dichalcogenide. *Nature Materials* **19**, 153–157 (2020).

18. Ko, K.-T. *et al.* RKKY Ferromagnetism with Ising-Like Spin States in Intercalated Fe1/4TaS2. *Physical Review Letters* **107**, (2011).

19. Fan, S. *et al.* Electronic chirality in the metallic ferromagnet Fe1/3TaS2. *Phys. Rev. B* **96**, 205119 (2017).

20. Mangelsen, S. *et al.* Large Anomalous Hall Effect and Slow Relaxation of the Magnetization in Fe1/3TaS2. *J. Phys. Chem. C* **124**, 24984–24994 (2020).

21. Ghimire, N. J. *et al.* Large anomalous Hall effect in the chiral-lattice antiferromagnet CoNb3S6. *Nature Communications* **9**, 3280 (2018).

22. Togawa, Y. *et al.* Chiral Magnetic Soliton Lattice on a Chiral Helimagnet. *Phys. Rev. Lett.* **108**, 107202 (2012).

23. Togawa, Y. *et al.* Interlayer Magnetoresistance due to Chiral Soliton Lattice Formation in Hexagonal Chiral Magnet CrNb3S6. *Phys. Rev. Lett.* **111**, 197204 (2013).

24. Mankovsky, S., Polesya, S., Ebert, H. & Bensch, W. Electronic and magnetic properties of 2H-NbS2 intercalated by 3d transition metals. *Phys. Rev. B* **94**, 184430 (2016).

25. Nakayama, M., Miwa, K., Ikuta, H., Hinode, H. & Wakihara, M. Electronic Structure of Intercalation Compounds of CoxNbS2. *Chem. Mater.* **18**, 4996–5001 (2006).

26. Zhang, C. *et al.* Critical behavior of intercalated quasi-van der Waals ferromagnet Fe0.26TaS2. *Phys. Rev. Materials* **3**, 114403 (2019).

27. Tenasini, G. *et al.* Giant anomalous Hall effect in quasi-two-dimensional layered antiferromagnet Co1/3NbS2. *Phys. Rev. Research* **2**, 023051 (2020).

28. Inui, A. *et al.* Chirality-Induced Spin-Polarized State of a Chiral Crystal CrNb3S6. *Phys. Rev. Lett.* **124**, 166602 (2020).

29. Parkin, S. S. P., Marseglia, E. A. & Brown, P. J. Magnetic structure of Co1/3NbS2and Co1/3TaS2. *J. Phys. C: Solid State Phys.* **16**, 2765–2778 (1983).

30. Korotin, Dm. *et al.* Construction and solution of a Wannier-functions based Hamiltonian in the pseudopotential plane-wave framework for strongly correlated materials. *Eur. Phys. J. B* **65**, 91 (2008).

31. Gainutdinov, I. I., Nemudry, A. P. & Zilberberg, I. L. Using Doping to Modify the Properties of SrFeO3 and SrCoO3 Oxides: DFT Calculations of the Electronic Structure. *J Struct Chem* **60**, 171–178 (2019).

32. Steurer, W. *et al.* Manipulation of the Charge State of Single Au Atoms on Insulating Multilayer Films. *Phys. Rev. Lett.* **114**, 036801 (2015).

33. Teichmann, K. *et al.* Bistable Charge Configuration of Donor Systems near the GaAs(110) Surfaces. *Nano Lett.* **11**, 3538–3542 (2011).

34. Kim, H., Chang, Y. H., Lee, S.-H., Kim, Y.-H. & Kahng, S.-J. Switching and Sensing Spin States of Co–Porphyrin in Bimolecular Reactions on Au(111) Using Scanning Tunneling Microscopy. *ACS Nano* **7**, 9312–9317 (2013).

35. Olsson, F. E., Paavilainen, S., Persson, M., Repp, J. & Meyer, G. Multiple Charge States of Ag Atoms on Ultrathin NaCl Films. *Phys. Rev. Lett.* **98**, 176803 (2007).

36. Hohenberg, P. & Kohn, W. Inhomogeneous Electron Gas. *Phys. Rev.* **136**, B864–B871 (1964).

37. Kresse, G. & Furthmüller, J. Efficient iterative schemes for ab initio total-energy calculations using a plane-wave basis set. *Phys. Rev. B* **54**, 11169–11186 (1996).

38. Kresse, G. & Furthmüller, J. Efficiency of ab-initio total energy calculations for metals and semiconductors using a plane-wave basis set. *Computational Materials Science* **6**, 15–50 (1996).

39. Kresse, G. & Hafner, J. Ab initio molecular-dynamics simulation of the liquid-metal–amorphous-semiconductor transition in germanium. *Phys. Rev. B* **49**, 14251–14269 (1994).

40. Perdew, J. P., Burke, K. & Ernzerhof, M. Generalized Gradient Approximation Made Simple. *Phys. Rev. Lett.* **77**, 3865–3868 (1996).

41. Blöchl, P. E. Projector augmented-wave method. *Phys. Rev. B* **50**, 17953–17979 (1994).

42. Mosey, N. J. & Carter, E. A. Ab initio evaluation of Coulomb and exchange parameters for DFT+U calculations. *Phys. Rev. B* **76**, 155123 (2007).

43. Monkhorst, H. J. & Pack, J. D. Special points for Brillouin-zone integrations. *Phys. Rev. B* **13**, 5188–5192 (1976).

44. Vanpoucke, D. E. P. & Brocks, G. Formation of Pt-induced Ge atomic nanowires on Pt/Ge(001): A density functional theory study. *Phys. Rev. B* **77**, 241308 (2008).

45. Haga, T., Fujimoto, Y. & Saito, S. Electronic structure and scanning tunneling microscopy images of heterostructures consisting of graphene and carbon-doped hexagonal boron nitride layers. *Phys. Rev. B* **100**, 125403 (2019).

Figures

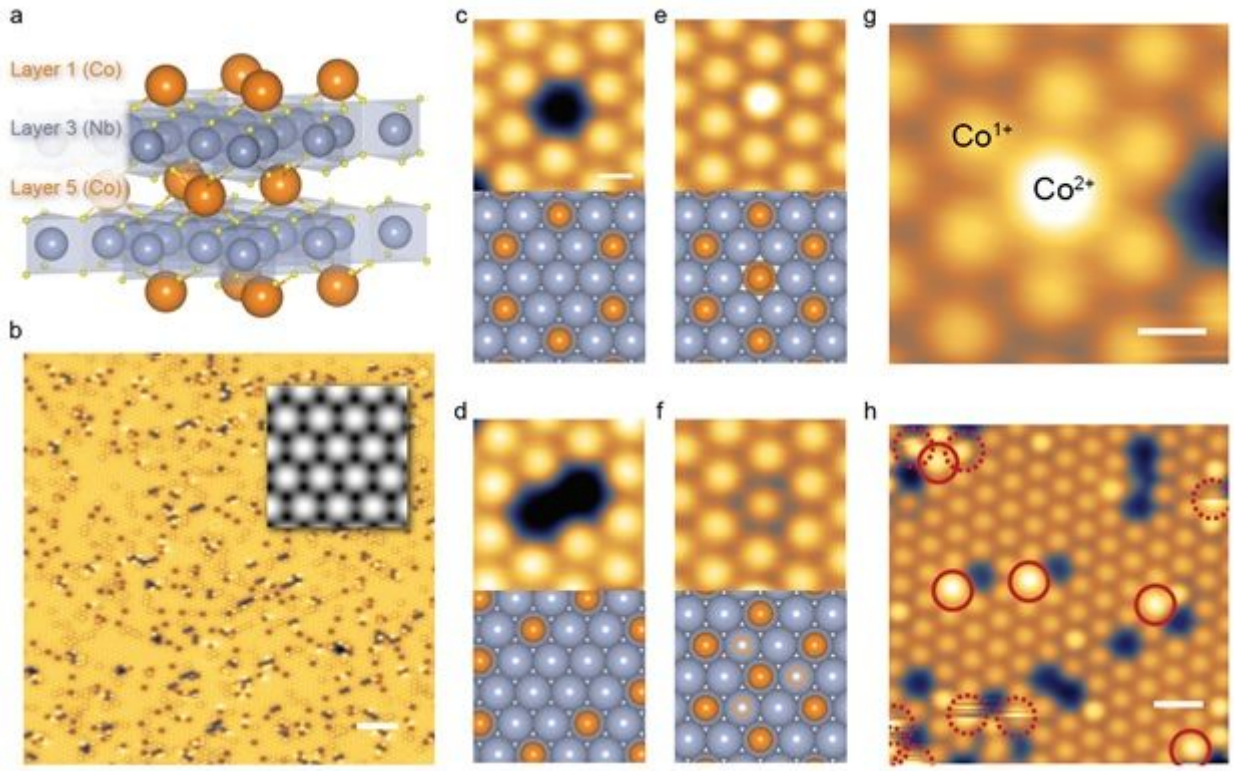

Figure 1

Various Structural Defects and Metastable Charged State from Cleaved Co1/3NbS2. a. Atomic structure of cleaved Co1/3NbS2. The exposed surface composed of intercalated Co and NbS2 matrix. Each layer is numbered from the surface into the bulk. b. STM image of a cleaved surface of Co1/3NbS2. (scale bar: 4 nm, inset: simulated STM image) c-f. STM image and atomic model of structural defects. (scale bar: 0.4 nm) c. Co monovacancy in layer 1. d. Co divacancy in layer 1. e. Co substitution of Nb in layer 3. f. Co trivacancy. The orange circles indicate the missing Co ions in layer 5. g. Metastable charged state, Co2+, showing a bright protrusion in STM image. (scale bar: 0.4 nm) h. Metastable charged states are indicated by red circles. Dashed red circles show the instability of the charged states near Co vacancies. (scale bar: 1 nm)

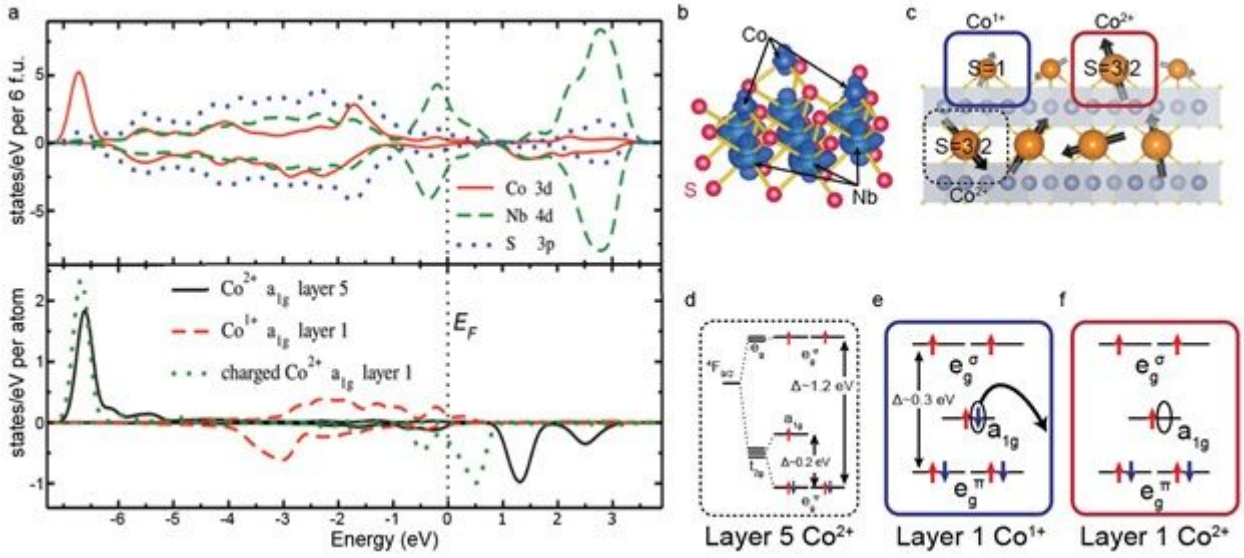

Figure 2

Change of Electron Density of States in the Metastable Charged Co2+ State. a. The total (top) and projected (bottom) electron density of states as obtained in DFT+U calculations. The positive and negative sign indicates projection to two opposite spin directions which reveals the non-compensated magnetic moment of Co. Nb 4d and S 3p states dominate the electron density near the Fermi level and are hybirized while Co a1g orbital band shows suppressed density of states. In the metastable charged state (Co2+ in layer 1), Co a1g orbital gets partially filled in and moves towards the Fermi energy. b. Electron density corresponding to the a1g-orbitals. c. Schematic showing the local magnetic moment of each Co configuration. d-f. Crystal field splitting diagrams of Co configurations. The (layer 1) surface configurations have reduced gap (egσ-t2g) from layer 5. The black circled electron states indicate the changing electron responsible for the formation of metastable charged state.

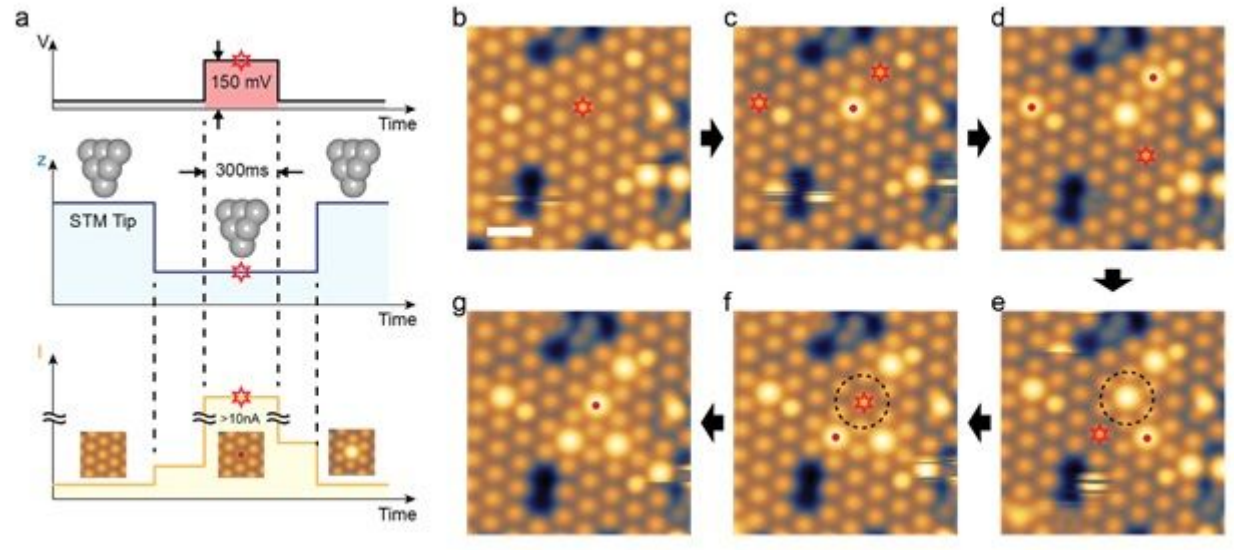

Figure 3

Manipulation of Metastable Charged State using a Voltage Pulse. a. Changes of voltage, tip height and tunneling current during the charging process. STM tip height is lowered by changing the feedback setpoint from 5pA to 100pA. After opening the feedback, voltage pulse of 150mV was applied for 300ms and the increased current was observed. Then the subsequent STM image shows a bright protrusion at the point. b-g. Series of STM images showing creation of charged Co2+ ions with STM pulses. Red stars indicate the positions where a voltage pulse is applied after the image was taken. The created charged Co2+ ions from the previous pulse are indicated by red points. During the process, one of the created Co2+ ions changed back to the ground state (black dashed circle) and has been applied a pulse one more time.

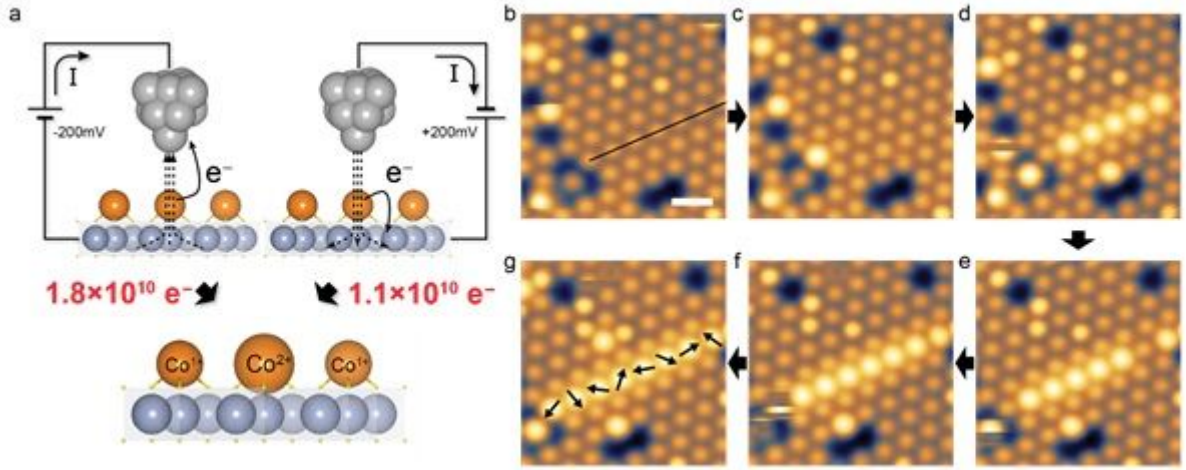

Figure 4

Formation of a S=3/2 Co2+ Linear Chain. a. Comparison of electron hopping direction in applying opposite bias polarity. An electron is moved from the target Co to the tip in the case of negative sample bias, and vice versa. The numbers of electrons to induce charging at a certain tunneling resistance (300

pA, ±200 mV) in both polarities are indicated by the numbers in red. b-g. Formation of a chain composed of eight S=3/2 Co2+ ions. STM pulses are applied along the black line in b and the first and seventh Co2+ ions were applied one more pulse since they went back to the ground state during the process. The charged Co ions appearing away from the line are not intended and are affected by the nearby defect configurations.

Supplementary Files

This is a list of supplementary files associated with this preprint. Click to download.

- Supplementary1.7.pdf